J. Fluid Mech. (1993), *vol.* 254, *pp.* 579–603

The role of acoustics in flame/vortex interactions

By T. L. JACKSON,[1] MICHÈLE G. MACARAEG[2] AND M. Y. HUSSAINI[3]

[1] Department of Mathematics and Statistics, Old Dominion University, Norfolk, VA 23529, USA

[2] NASA Langley Research Center, Hampton, VA 23681-0001, USA

[3] Institute for Computer Applications in Science and Engineering, NASA Langley Research Center, Hampton, VA 23681-0001, USA

(Received 11 March 1992 and in revised form 7 April 1993)

The role of acoustics in flame/vortex interactions is examined via asymptotic analysis and numerical simulation. The model consists of a one-step, irreversible Arrhenius reaction between initially unmixed species occupying adjacent half-planes which are allowed to mix and react by convection and diffusion in the presence of an acoustic field or a time-varying pressure field of small amplitude. The main emphasis is on the influence of the acoustics on the ignition time and flame structure as a function of vortex Reynolds number and initial temperature differences of the reactants.

1. Introduction

Acoustic waves play a pervasive role in compressible flows even in the low Mach number limit. They are a necessary concomitant of nonlinear interactions such as those present in turbulent flows. For instance, the interaction of any disturbance, whether it is of the entropy or the vorticity type, with steep gradients as in shocked flows (e.g. McKenzie & Westphal 1968; Zang, Hussaini & Bushnell 1984) generates acoustic waves. Chemical reactions enhance them (Toong *et al.* 1974; Robert 1978; Clarke 1985; Jackson, Hussaini & Ribner 1993). Conversely, acoustic waves can engender instability in laminar shear flows which may eventually suffer transition to turbulence (Goldstein & Hultgren 1989). In reactive flows, they play a similar critical role. It is now well established that they can significantly affect the stability of flames (McIntosh 1986), the transition to detonation (Urtiew & Oppenheim 1966; Lee 1977; Shepherd & Lee 1992), etc. Oran & Gardner (1985) provide a fine review of combustion–acoustics interactions with an emphasis on the physics rather than the mathematical analysis and techniques.

In the present study, the role of acoustics in the flame/vortex interaction process is investigated. In order to provide a proper perspective, the literature on the flame/vortex interaction problem is briefly reviewed here. This problem was first formulated by Marble (1985) to model one of the basic physical mechanisms underlying the complex processes of turbulent diffusion flames or combustion in vortex-dominated flows. The model consists of a diffusion flame with fast chemical kinetics (along the horizontal axis separating two reactants occupying the upper and lower half-planes) which is distorted by a vortex with its centre at the origin. The theoretical results have established that the flame sheet is rolled up into a spiral around the vortex on the convection timescale, forming a reacted core, and then spreads across the spirals on the diffusion timescale; the growth rate of the reacted viscous core obeys a similarity law, and so does the reactant-consumption rate which is independent of

time. These physical features are confirmed by numerical simulations (Laverdant & Candel 1988; Rehm *et al.* 1989; Norton 1983) implying, thereby, that the inclusion of shear (which was neglected by Marble) or finite-rate chemistry does not alter the qualitative picture. The premixed combustion in a vortex also displays similar features (Peters & Williams 1988).

The aforementioned studies assume the simultaneous existence of a flame and a vortex and the subsequent evolution. Thus, they preclude ignition regime which is the main thrust of Macaraeg, Jackson & Hussaini's (1992) work. Their work is based on the assumption of a constant-density, one-step Arrhenius reaction between the fuel and the oxidizer, occupying adjacent half-spaces, in the presence of a vortex with its centre on the axis of demarcation between the reactants. Their study focuses on the ignition time, location and the flame structure as a function of the vortex Reynolds number and the initial temperature differences of the reactants. In the absence of the vortex, the problem, of course, reduces to the classical case of Linan & Crespo (1976) who analysed the continuous temporal evolution of such a configuration from nearly frozen flow to near equilibrium flow. The reactants mix by diffusion until, at some finite time, a thermal explosion occurs at a well-defined location, and ignition takes place. After ignition, a pair of deflagration waves (or premixed flamelets) emerges according to classical thermal explosion theory. These premixed flamelets are quite weak in that the temperature rise associated with them is small, and they exist only until all of the deficient reactant is consumed. Just beyond the deflagration waves, a diffusion flame regime exists where the mixing process is governed by diffusion in the direction normal to the flame. As time increases, the diffusion flame approaches a flame sheet. We note that the existence of a well-defined ignition point and the premixed flamelets depends critically on the relative magnitudes of the two initial temperatures to that of the adiabatic diffusion flame temperature. That is, if the adiabatic diffusion flame temperature is greater than either initial temperature, a well-defined ignition point always occurs, followed by the premixed flamelets. On the other hand, if the adiabatic diffusion flame temperature is between the two initial temperatures, there is no well-defined ignition point, and a single premixed flame merges smoothly into the diffusion flame. This configuration of a triple-flame (or tribrachial flame) appears to be of such a fundamental nature that it also exists in steady supersonic reacting laminar mixing layers (e.g. Jackson & Hussaini 1988; Grosch & Jackson 1991) and flames propagating into a non-uniform mixture (e.g. Buckmaster & Matalon 1988; Dold 1989; Hartley & Dold 1991).

The initial presence of a vortex alters the picture considerably (Macaraeg *et al.* 1992). First, a hot spot develops within the viscous core of the vortex and evolves into an almost circular flame which grows with time according to a similarity rule and so does the reactant-consumption rate, as in the case of Marble. Next, the Linan & Crespo scenario or the tribrachial flame configuration must evolve at infinite distance to the right and left of the origin. The diffusion flames emanating from this configuration then move toward and finally merge with the flames in the reacted core region. The above picture is only valid for the case when the adiabatic flame temperature is greater than either of the two initial temperatures. When the adiabatic flame temperature lies between the initial temperatures, a well-defined ignition point does not occur, but rather the premixed region merges smoothly into the diffusion flame region, independent of the vortex Reynolds numbers. This scenario is consistent with the Linan & Crespo analysis.

The presence of an acoustic field or time-dependent pressure perturbation affects both the ignition and the flame structure. To investigate the ignition regime, an

asymptotic theory is developed here which holds strictly for near-equal temperatures of the reactants. For low frequencies of a time-periodic pressure perturbation, ignition can be accelerated or significantly delayed depending on the phase. For moderate to high frequencies ignition is always enhanced. An approximation based on homogeneous ignition theory is given which predict these trends very well, and therefore is proposed as a good engineering approximation for obtaining the ignition times for the more complicated flow fields. For the complete time evolution from nearly frozen flow to near equilibrium flow, an asymptotic analysis based on small heat release is employed. In this limit, direct simulations show that acoustics have little effect on the flow field in the vortex core, while the flow outside the core oscillates. It is believed that viscosity in the reacted core damps out the acoustic field.

In the next section the problem is formulated. Section 3 presents an analysis of the ignition regime, valid only for near-equal initial temperatures of the reactants, using a combination of large activation energy (and hence, large Zeldovich number) asymptotics and numerics for several different pressure profiles. The pressure profiles chosen are either a linear, or a pulse, or a sinusoidal function. This last case is stressed since it represents a single Fourier component of a more general pressure disturbance. Also in this section, the approximation based on the homogeneous ignition theory is presented. Section 4 presents selected numerical results of the continuous evolution from nearly frozen flow to near equilibrium flow for the sinusoidal pressure profile under the assumption of small heat release. A description of the diffusion flame regime is given in §5 and our conclusions are presented in §6.

2. Problem formulation

In this section the problem of the time evolution of initially unmixed species occupying adjacent half-planes which are then allowed to mix and react in the presence of a vortex subject to pressure disturbance is formulated. The non-dimensional equations governing this field, assuming constant viscous and thermodynamic properties, are given by Buckmaster & Ludford (1982) and Williams (1985):

$$\rho T = 1+\delta P_c(t)+\gamma M^2\bar{P}(x,y,z,t), \tag{2.1a}$$

$$\rho_t+(\rho u)_x+(\rho v)_y+(\rho w)_z = 0, \tag{2.1b}$$

$$\rho[u_t+uu_x+vu_y+wu_z]+\bar{P}_x = Sc(\nabla^2 u+\tfrac{1}{3}K_x), \tag{2.1c}$$

$$\rho[v_t+uv_x+vv_y+wv_z]+\bar{P}_y = Sc(\nabla^2 v+\tfrac{1}{3}K_y), \tag{2.1d}$$

$$\rho[w_t+uw_x+vw_y+ww_z]+\bar{P}_z = Sc(\nabla^2 w+\tfrac{1}{3}K_z), \tag{2.1e}$$

$$\rho[T_t+uT_x+vT_y+wT_z]-\delta\frac{\gamma-1}{\gamma}\frac{\mathrm{d}P_c}{\mathrm{d}t}$$
$$-(\gamma-1)M^2[\bar{P}_t+u\bar{P}_x+v\bar{P}_y+w\bar{P}_z] = \nabla^2 T+(\gamma-1)M^2 Sc\,\Phi+\beta\Omega, \tag{2.1f}$$

$$\rho[F_{j,t}+uF_{j,x}+vF_{j,y}+wF_{j,z}] = \nabla^2 F_j-\Omega, \quad j=1,2, \tag{2.1g}$$

$$\Omega = Da\,\rho F_1 F_2 \mathrm{e}^{-Ze/T}, \tag{2.1h}$$

where $K = u_x+v_y+w_z$, Φ is the viscous dissipation term, and ∇^2 is the three-dimensional Laplacian operator. Here, (u,v,w) are the velocity components in the (x,y,z) directions, respectively; ρ is the density; T is the temperature; and F_1 and F_2 the mass fractions of the fuel and oxidizer, respectively. The total pressure $P = 1+\delta P_c+\gamma M^2\bar{P}$ is written as the sum of the compressible component P_c plus

incompressible component $\bar{P}$, as is consistent with the small-Mach-number approximation (e.g. Majda 1984), with δ the amplitude of the compressible component. The actual size of δ will be chosen in the course of the analysis. The chemical model is assumed to be a one-step, irreversible Arrhenius reaction. The non-dimensional parameters appearing above are the Schmidt number $Sc = \nu/D$ assumed equal for both species, with D the species diffusion coefficient and ν the kinematic viscosity; the Zeldovich number $Ze = E/(R^0 T_\infty)$, with E the dimensional activation energy and R^0 the universal gas constant; the Damköhler number Da, defined as the ratio of the characteristic timescale t_c to the characteristic reaction timescale t_R; γ the ratio of specific heats; and finally β the heat release per unit mass of $F_{1,\infty}$. In specifying the Damköhler number in the course of the analysis, the appropriate choice for the characteristic timescale is made. The density, temperature, pressure and mass fractions were non-dimensionalized by their initial values ρ_∞, T_∞, $P_\infty = \rho_\infty R^0 T_\infty$ and $F_{1,\infty}$, respectively, that would prevail if there were no pressure disturbances. The Lewis number was assumed to be unity, which implies that $Sc = Pr$, where $Pr = \rho_\infty C_p \nu/\lambda$ is the Prandtl number, λ is the thermal conductivity and C_p is the specific heat at constant pressure. Lengths and velocities are referred to the relevant diffusion characteristic scales $l_d^2 = Dt_c$ and $U_d = l_d/t_c$, respectively. In this case, the Reynolds number based on this choice of l_d and U_d is given by $Re = l_d U_d/\nu = 1/Sc$. The Mach number M is defined as U_d/a_∞, the ratio of the characteristic diffusion speed to the speed of sound. The above choices for t_c, l_d, and U_d are consistent with the scales chosen in the absence of a vortex.

An analysis of the ignition zone with acoustic interactions must take into account the two fundamental ratios

$$\tau = \frac{\text{characteristic time}, t_c}{\text{acoustic time}, t_a} = \frac{l_d/U_d}{l_a/a_\infty},$$

$$N = \frac{\text{characteristic acoustic length}}{\text{diffusion length}} = \frac{l_a}{l_d}.$$

Thee two ratios are related via

$$\tau = 1/NM,$$

where M is the Mach number defined above. Here, our analysis is based on the assumption that $\tau = O(1)$, and hence the acoustic wavelength is much longer than the characteristic diffusion lengthscale for small Mach numbers. Thus, the pressure gradient within the combustion zone is negligibly small and the pressure is essentially a function of time, and so the flame is treated as isobaric to an excellent approximation. In addition, our analysis further assumes that the magnitude of the acoustic time relative to the reaction time is given by

$$Da = \frac{\text{characteristic time}, t_c}{\text{reaction time}, t_R} \equiv \tau \frac{t_a}{t_R}.$$

Taking $\tau = O(1)$, we shall assume that the reaction time is much faster than the acoustic time, and so we take the Damköhler number to be proportional to

$$Da \approx \frac{\mathrm{e}^{Ze}}{Ze},$$

where $Ze \gg 1$ is the Zeldovich number defined above, thus defining the characteristic

time. The exact form is chosen in the course of the analysis. In our analysis, if the Mach number M was not chosen small, we would also need to consider spatial variations of the pressure disturbance inside the reaction zone.

It should be noted that, for compressible flows, spatial variations of the pressure disturbance must be taken into account. This leads to the well known Kapila–Clarke equation in which thermal runaway occurs somewhere between the constant-pressure case and the constant-volume case. Here, the characteristic length l_d is but a fraction of the acoustic wavelength l_a in the limit of zero Mach number, so that pressure variations across the region studied are small and the flame can be treated as isobaric to a good approximation. Thus, our analysis is essentially incompressible, and so the explosion is always close to the constant-pressure case. Indeed, for the constant-volume case (i.e. $\rho_1 = 0$), the gas law (3.3a) shows that $T_1 = P_c/\gamma - 1$, and since P_c is known and fixed from the outside acoustic field, the temperature perturbation can never become unbounded, contradicting the fact that ignition must take place. This, of course, is not the case when the Mach number is $O(1)$, since the pressure perturbation can become unbounded. A relevant discussion of the different scales involved, and the proper conditions in which the Clarke–Kapila equation can arise, can be found in Kassoy, Kapila & Stewart (1989).

McIntosh (1986, 1989, 1991 and McIntosh & Wilce 1991, and the references cited therein) pointed out the importance of the two fundamental ratios given above when the characteristic velocity is given by the flame speed U_f. For this case, three distinct cases of flame–acoustic interactions arise depending on the magnitude of τ, and there have been classified in McIntosh (1991). Further phenomena can exist depending on the magnitude of the acoustic time/reaction time ratio, and a discussion of this can be found in Clarke (1985). For $\tau = O(1)$, McIntosh & Wilce (1991) point out that audible sound and its interference with flames would come under this category, and a considerable body of work exists using this assumption (e.g. references cited therein).

We shall now assume that the flow is independent of the downstream direction x for all time. Although not true for any real flow situation, it is consistent with experimental observations that streamwise vortical structures in turbulent mixing layers are essentially aligned with the flow and are of great extent. Also, neglecting the x-dependency can be thought of as a local approximation for the vortices found in turbulent flames. This type of approximation has also been used previously in describing the evolution of a shear flow with an embedded streamwise vortex (Corcos 1988; Pearson & Abernathy 1984). We shall also assume that the Mach number is small, as is typical for flames (e.g. Buckmaster & Ludford 1982; Williams 1985). Thus, the governing equations (2.2), in the limit of small Mach number and neglecting all dependency in x, reduce to

$$\rho T = 1 + \delta P_c(t), \tag{2.2a}$$

$$\rho_t + (\rho v)_y + (\rho w)_z = 0, \tag{2.2b}$$

$$\rho[u_t + vu_y + wu_z] = Sc\,\nabla^2 u, \tag{2.2c}$$

$$\rho[v_t + vv_y + wv_z] + \bar{P}_y = Sc(\nabla^2 v + \tfrac{1}{3}K_y), \tag{2.2d}$$

$$\rho[w_t + vw_y + ww_z] + \bar{P}_z = Sc(\nabla^2 w + \tfrac{1}{3}K_z), \tag{2.2e}$$

$$\rho[T_t + vT_y + wT_z] - \delta\frac{\gamma-1}{\gamma}\frac{\mathrm{d}P_c}{\mathrm{d}t} = \nabla^2 T + \beta\Omega, \tag{2.2f}$$

$$\rho[F_{j,t} + vF_{j,y} + wF_{j,z}] = \nabla^2 F_j - \Omega, \quad j = 1, 2, \tag{2.2g}$$

where $\nabla^2 = (\,)_{yy} + (\,)_{zz}$ is the two-dimensional Laplacian operator, $K = v_y + w_z$, and

we have considered the distinguished limit $M^2 \ll \delta \ll 1$. Since we are interested in reacting flows with vortical motion, we transform (2.2) into cylindrical coordinates $(y, z) \to (r, \theta)$ by using the transformations $y = r\cos\theta$ and $z = r\sin\theta$. If we define g to be the radial velocity and h to be the tangential velocity, i.e. $v = g\cos\theta - h\sin\theta$ and $w = g\sin\theta + h\cos\theta$, then (2.2) transforms to

$$\rho T = 1 + \delta P_c(t), \tag{2.3a}$$

$$\rho_t + (\rho g)_r + \frac{1}{r}(\rho h)_\theta + \frac{\rho g}{r} = 0, \tag{2.3b}$$

$$\rho\left[u_t + g u_r + \frac{h}{r}u_\theta\right] = Sc\,\nabla^2 u, \tag{2.3c}$$

$$\rho\left[g_t + g g_r + \frac{h}{r}g_\theta - \frac{h^2}{r}\right] + \bar{P}_r = Sc\left(\nabla^2 g - \frac{g}{r^2} - \frac{2}{r^2}h_\theta + \tfrac{1}{3}K_r\right), \tag{2.3d}$$

$$\rho\left[h_t + g h_r + \frac{h}{r}h_\theta + \frac{gh}{r}\right] + \frac{1}{r}\bar{P}_\theta = Sc\left(\nabla^2 h - \frac{h}{r^2} + \frac{2}{r^2}g_\theta + \frac{1}{3r}K_\theta\right), \tag{2.3e}$$

$$\rho\left[T_t + g T_r + \frac{h}{r}T_\theta\right] - \delta\frac{\gamma-1}{\gamma}\frac{\mathrm{d}P_c}{\mathrm{d}t} = \nabla^2 T + \beta\Omega, \tag{2.3f}$$

$$\rho\left[F_{j,t} + g F_{j,r} + \frac{h}{r}F_{j,\theta}\right] = \nabla^2 F_j - \Omega, \quad j = 1, 2, \tag{2.3g}$$

where ∇^2 is now the two-dimensional Laplacian operator in cylindrical coordinates, and $K = g_r + g/r + h_\theta/r$. The system (2.3) must be solved subject to appropriate boundary and initial conditions.

Since it is known that small pressure disturbances of $O(Ze^{-1})$ can cause $O(1)$ changes in certain flame properties such as the burning rate, extinction, transition from laminar to turbulence, etc. (Buckmaster & Ludford 1982; Buckmaster 1992; Kapila 1992), we shall limit our attention to small pressure disturbances by defining for the total pressure

$$P = 1 + Ze^{-1}\frac{\gamma}{\gamma-1}P_c(t) + O(M^2), \quad \delta = \frac{\gamma}{\gamma-1}Ze^{-1}; \tag{2.4}$$

the factor $\gamma/(\gamma-1)$ in the definition of δ was chosen for convenience. Thus, we are concerned with $O(Ze^{-1})$ acoustic perturbations superimposed on a basic state. The pressure perturbation $P_c(t)$ can be determined by solving the acoustic equations in the outer field (e.g. Van Harten, Kapila & Matkowsky 1984), and indicates that the pressure can be controlled, for example, from the surroundings. A general expression for P_c can be found in Majda (1984) and will depend on the type of conditions imposed on the geometry under consideration. Since we are interested in the influence of pressure variations on the flame, we will not solve this outer problem and, henceforth, consider the pressure disturbance P_c to be prescribed.

We note here that it is the density that couples the momentum equations to the temperature and mass fraction equations. As such, the numerical solution to the full system (2.3) is a formidable task. One approximation that will simplify (2.3) to a more tractable system is the assumption of small heat release (e.g. Van Harten *et al.* 1984). The resulting system can then be solved numerically, and will be presented in §4. For the ignition problem, the assumption of small heat release is not needed in order to

simplify the system, provided that we restrict the analysis to near-equal initial temperatures, and hence densities, of the two gases. This analysis is presented in the following section.

3. Ignition

At time $t = 0$, the reaction rate is exactly zero owing to the product $F_1 F_2 = 0$. For $t > 0$, the fuel and oxidizer begin to mix by diffusion, as well as by convection due to the presence of the vortex, and the reaction rate is no longer zero. For small time, it can thus reasonably be assumed that the effect of the reaction on the overall flow field is small. The solution for small time in which the reaction rate term is neglected is known as the inert or chemically frozen solution, and will be denoted by the superscript I. In what follows, we only consider the case of near-equal initial temperatures. This assumption leads to the inert solutions $T^I = \rho^I = 1 + O(Ze^{-1})$, where the $O(Ze^{-1})$ term is included to allow for small initial temperature differences that might exist in the absence of any pressure disturbances. Thus, the leading-order inert solution corresponds to the constant-density approximation prevalent in the combustion literature. As time increases, more of the combustible mixes until, at some finite time, a thermal explosion occurs characterized by significant departure from the inert. To analyse the ignition process, we determine the effect of the growing reaction rate by expanding about the inert solution as

$$T = 1 + Ze^{-1}[T_1 + P_c(t)] + O(Ze^{-2}), \quad \rho = 1 + Ze^{-1}\rho_1 + O(Ze^{-2}), \quad F_j = F_j^I + O(Ze^{-1}), \tag{3.1}$$

$$u = u^I + O(Ze^{-1}), \quad g = g^I + O(Ze^{-1}), \quad h = h^I + O(Ze^{-1}), \tag{3.2}$$

and take the asymptotic limit $Ze \to \infty$. The leading-order equations are given by

$$\rho_1 + T_1 = \frac{1}{\gamma - 1} P_c(t), \tag{3.3a}$$

$$g_r^I + \frac{1}{r} h_\theta^I + \frac{g^I}{r} = 0, \tag{3.3b}$$

$$u_t^I + g^I u_r^I + \frac{h^I}{r} u_\theta^I = Sc \nabla^2 u^I, \tag{3.3c}$$

$$g_t^I + g^I g_r^I + \frac{h^I}{r} g_\theta^I - \frac{h^{I^2}}{r} + \bar{P}_r = Sc\left(\nabla^2 g^I - \frac{g^I}{r^2} - \frac{2}{r^2} h_\theta^I\right), \tag{3.3d}$$

$$h_t^I + g^I h_r^I + \frac{h^I}{r} h_\theta^I + \frac{g^I h^I}{r} + \frac{1}{r} \bar{P}_\theta = Sc\left(\nabla^2 h^I - \frac{h^I}{r^2} + \frac{2}{r^2} g_\theta^I\right), \tag{3.3e}$$

$$T_{1,t} + g^I T_{1,r} + \frac{h^I}{r} T_{1,\theta} = \nabla^2 T_1 + A F_1^I F_2^I \, e^{T_1 + P_c(t)}, \tag{3.3f}$$

$$F_{j,t}^I + g^I F_{j,r}^I + \frac{h^I}{r} F_{j,\theta}^I = \nabla^2 F_j^I, \quad j = 1, 2, \tag{3.3g}$$

where we have chose the Damköhler number Da to be

$$Da = \frac{A}{\beta Ze} e^{Ze}, \tag{3.4}$$

and A is some constant that will be chosen in the course of the analysis. This particular choice of the Damköhler number ensures that a distinguished limit exists, in that the reaction rate term is of the same order in a Zeldovich number expansion as the time derivative terms (see e.g. Buckmaster & Ludford 1982). Note that the pressure disturbance now appears in the exponential and thus will play a crucial role in the ignition process.

We first see that the continuity and momentum equations (3.3*b–e*) are decoupled from the rest of the system and thus will completely determine u^I, g^I, h^I *and* $\bar{P}$. At $t = 0$, we situate a point vortex at the origin and allow it to diffuse under the action of viscosity. Then, assuming the flow in the (r, θ)-plane to be axisymmetric, the induced flow field is given by (Lamb 1932)

$$g^I = 0, \quad h^I = \frac{R\,Sc}{r}[1 - e^{-r^2/4t\,Sc}], \tag{3.5}$$

$$\bar{P}(r, t) = -\int_r^\infty \frac{h^{I^2}(\bar{r}, t)}{\bar{r}}\,d\bar{r}, \tag{3.6}$$

and u^I is found from the equation

$$u^I_t + \frac{h^I}{r}u^I_\theta = Sc\,\nabla^2 u^I. \tag{3.7}$$

The solution (3.5)–(3.6) is the solution for the incompressible Oseen vortex, where $R = \Gamma/2\pi\nu$ is the vortex Reynolds number and Γ is the circulation parameter. The vortex Reynolds number R is considered as a free parameter and its choice determines the importance of the vortex in the initial mixing of the reactants. When $R = 0$ (i.e. $\Gamma = 0$), there is no vortex and the initially separated reactant mix by diffusion only. When the vortex Reynolds number R is non-zero, the initially separated reactants mix by diffusion and convection. The solution to (3.7) has been discussed previously in the context of streamwise–spanwise vorticity interactions for non-reacting flows (Corcos 1988; Pearson & Abernathy 1984). Note that u^I does not appear in the temperature or mass fraction equations since we neglected variations in x coupled with the zero-Mach-number approximation, and so the analysis is valid for either streamwise or spanwise vortices. The velocity component u^I will influence the temperature equation if true compressibility effects are taken into account; this will necessarily occur after ignition has taken place.

With g^I and h^I now known, the following equations can be solved for T_1 and F^I_j:

$$T_{1,t} + \frac{h^I}{r}T_{1,\theta} = \nabla^2 T_1 + AF^I_1 F^I_2 e^{T_1 + P_c(t)}, \tag{3.8}$$

$$F^I_{j,t} + \frac{h^I}{r}F^I_{j,\theta} = \nabla^2 F^I_j, \quad j = 1, 2. \tag{3.9}$$

The appropriate boundary and initial conditions are given by

$$T_1 = 0, F^I_1 = 1, F^I_2 = 0 \quad \text{at} \quad t = 0, r > 0, 0 < \theta < \pi, \quad \text{and} \quad t > 0, r \to \infty, 0 < \theta < \pi, \tag{3.10a}$$

$$T_1 = \beta_T, F^I_1 = 0, F^I_2 = \frac{F_{2,-\infty}}{F_{1,\infty}} \equiv \phi^{-1} \quad \text{at} \quad t = 0, r > 0, \pi < \theta < 2\pi,$$

$$\text{and} \quad t > 0, r \to \infty, \pi < \theta < 2\pi, \tag{3.10b}$$

where ϕ is the equivalence ratio defined as the ratio of the initial mass fraction of the fuel $F_{1,\infty}$ to the initial mass fraction of the oxidizer $F_{2,-\infty}$ and β_T is the parameter that allows for small initial temperature differences in the absence of pressure disturbances. If $\phi = 1$, the mixture is said to be stoichiometric; if $\phi > 1$ it is fuel rich; and if $\phi < 1$, it is fuel lean. Also, if β_T is less than zero, the oxidizer (species 2) is relatively cold compared to the fuel (species 1); and if β_T is greater than zero, it is relatively hot. As t increases, the solution for T_1 becomes unbounded at some finite time (t_{ig}) and location (y_{ig}, z_{ig}). This characterizes the ignition regime. The special case $R = 0$, in which two initially unmixed species are allowed to diffuse without the mixing generated by the vortex, will be discussed in §3.1, while the case for $R > 0$ will be presented in §3.2. Finally, with T_1 determined, the density perturbation ρ_1 can be found from (3.3*a*).

3.1. $R = 0$

In the absence of any vortical motion, the governing equations reduce to the reactive–diffusive equations

$$T_{1,t} = T_{1,zz} + AF_1^I F_2^I \mathrm{e}^{T_1 + P_c(t)}, \tag{3.11}$$

$$F_{j,t}^I = F_{j,zz}^I, \quad j = 1, 2, \tag{3.12}$$

subject to the boundary and initial conditions

$$T_1 = 0, F_1^I = 1, F_2^I = 0 \quad \text{at} \quad t = 0, z > 0 \quad \text{and} \quad t > 0, z \to \infty, \tag{3.13a}$$

$$T_1 = \beta_T, F_1^I = 0, F_2^I = \phi^{-1} \quad \text{at} \quad t = 0, z < 0 \quad \text{and} \quad t > 0, z \to -\infty. \tag{3.13b}$$

The parabolic equations for the mass fractions can be integrated to yield

$$F_1^I = \Psi, F_2^I = \phi^{-1}(1 - \Psi), \tag{3.14}$$

where

$$\Psi = \tfrac{1}{2}(1 + \operatorname{erf}\eta), \tag{3.15}$$

and η is the similarity variable, defined as

$$\eta = \frac{z}{2t^{\frac{1}{2}}}. \tag{3.16}$$

Upon substituting the inert solutions into the temperature perturbation equation, and transforming to the similarity plane, a single equation for T_1 emerges, given by

$$4tT_{1,t} - T_{1,\eta\eta} - 2\eta T_{1,\eta} = 4t\Psi(1 - \Psi)\mathrm{e}^{T_1 + P_c(t)}, \tag{3.17}$$

which must be solved numerically subject to the boundary and initial conditions

$$T_1 = 0 \quad \text{at} \quad t = 0, z > 0 \quad \text{and} \quad T > 0, z \to \infty, \tag{3.18a}$$

$$T_1 = \beta_T \quad \text{at} \quad t = 0, z < 0 \quad \text{and} \quad T > 0, z \to -\infty. \tag{3.18b}$$

Here, the constant A appearing in the definition of the Damköhler number has been chosen to be ϕ for convenience. The special case of no pressure disturbance ($P_c = 0$) corresponds to the results of Linan & Crespo (1976) which has been discussed in the Introduction. Thus, the results of this subsection can be thought of as an extension of the Linan & Crespo problem to include pressure disturbances. In the following subsections we will select three different pressure variations, and compare with the results of Linan & Crespo. The first two choices for the pressure variation presented below correspond to the choices taken by Ledder & Kapila (1991) in their study of the

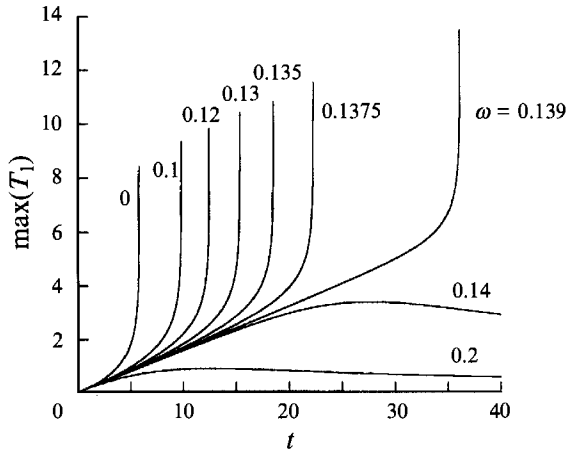

FIGURE 1. Plot of the maximum of the temperature perturbation T_1 as a function of time t for several values of ω and for $\beta_T = 0$. Linear pressure profile.

response of premixed flames to pressure perturbations. The last choice will be a sinusoidal pressure variation, which represents a single Fourier component of a more general pressure disturbance.

3.1.1. *Linear pressure decrease*

Let the flow be subject to a linear pressure decrease at $t = 0$ of the form

$$P_c(t) = -\omega t, \tag{3.19}$$

where $1/\omega > 0$ characterizes the timescale of the pressure disturbance. The influence of this linear pressure profile on premixed flames has been discussed by Ledder & Kapila (1991), in which extinction was seen to occur for all values of ω. This profile was chosen for this study because of its simplicity in form in that the ignition time and location will only be a function of the parameters ω and β_T, and also may represent the first term in a Taylor series expansion of a more general pressure disturbance. Figure 1 is a plot of the maximum of T_1 versus t for several values of ω and $\beta_T = 0$. The case $\omega = 0$ corresponds to that of Linan & Crespo (1976) in which no pressure disturbance is present. As ω is increased from zero, the ignition time also increases until, at some finite value $\omega \equiv \omega_c \approx 0.1395$, the ignition time is pushed to infinity. Thus, small values of ω can significantly delay ignition. For values of ω greater than ω_c, the maximum T_1 initially increases, reaches a maximum, then begins to decrease back to zero as time increases further. Thus, ignition does not occur in the classical sense. Mathematically, when the pressure disturbance becomes large and negative, the nonlinear source term of (3.17) becomes exponentially small and so can be neglected; T_1 then evolves according to a homogeneous heat equation. Although the solution of this system suggests that ignition will not occur for ω greater than ω_c, we note that the presence of an infinite amount of fuel and oxidizer necessitate that ignition will eventually take place. Asymptotically, the expansion (2.4) breaks down when t is of $O(Ze)$, and a new expansion must be employed, one which allows $O(1)$ changes in the pressure and the temperature; the waves now cease to be acoustic in nature. The leading-order system in this case is no longer that with constant density and, hence, the full system (2.3) must be solved numerically. This numerical problem is beyond the scope of the present study. Figure 2 is a plot of the ignition time t_{ig} versus ω for three values of the

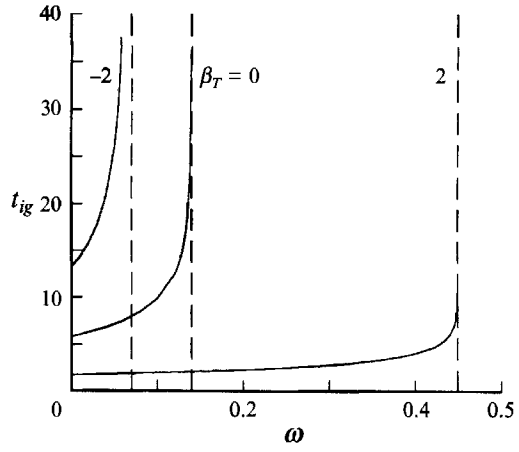

FIGURE 2. Plot of the ignition time t_{ig} as a function of ω for several values of β_T. Linear pressure profile.

temperature ratio parameter β_T. The case of $\beta_T = 0$ was presented in a slightly different manner in figure 1. Here, it is clear that as ω approaches 0.1395 from below, the ignition time goes to infinity, and for ω greater than 0.1395 there is no ignition. The case $\omega = 0$ corresponds to that of Linan & Crespo (1974); ignition time increases as β_T is decreased from zero ($F_{2,\infty}$ is relatively cold compared to $F_{1,\infty}$), and decreases as β_T is increased from zero. For each value of the temperature-ratio parameter, a critical value of ω is seen to exist; this value being less than 0.1395 for negative β_T and greater than 0.1395 for positive values of β_T. In the absence of any pressure disturbance, Linan & Crespo has shown that ignition takes place along a line parallel to the y-axis which is located at $z_{ig} = 0$ for $\beta_T = 0$ and resides in the hotter region for $\beta_T \neq 0$. In the presence of the linear pressure disturbance and for $\beta_T = 0$, ignition always occurs along the line $z_{ig} = 0$ for any value of ω. However, for $\beta_T \neq 0$, the ignition line $z = z_{ig}$ ($z_{ig} < 0$ for $\beta_T > 0$, and $z_{ig} > 0$ for $\beta_T < 0$) moves toward the line $z = 0$ as ω is increased.

3.1.2. *Pressure pulse*

Let the flow be subject to a pressure pulse at $t = 0$ of the form

$$P_c(t) = 4P_A(2^{-\omega t^2} - 2^{-2\omega t^2}), \tag{3.20}$$

where $\omega^{-\frac{1}{2}} > 0$ is the pulse width and $|P_A|$ is the amplitude of the pressure pulse. This corresponds to a smooth increase beginning at zero, increasing or decreasing to an extremum $|P_A|$ at $\omega t^2 = 1$, and finally returning to zero. The influence of this pressure pulse on premixed flames has been discussed by Ledder & Kapila (1991), in which extinction is seen to occur for both negative and positive amplitudes, depending upon the parameters of the problem. Figure 3 is a plot of ignition time t_{ig} versus ω for various values of the amplitude P_A with $\beta_T = 0$. The case of $P_A = 0$ corresponds to that of Linan & Crespo (1976) and is shown in the figure as a dashed line for reference. In addition, all data curves shown in this figure begin at $t_{ig} = 5.8285$ at $\omega = 0$, again consistent with the results of Linan & Crespo. For fixed $P_A < 0$, the ignition time initially increases as ω increases from zero, reaches a maximum, and then begins to decrease as ω is increased further, reaching an asymptote as $\omega \to \infty$. For fixed ω, decreasing the pressure amplitude from zero increases the ignition time. Thus, ignition

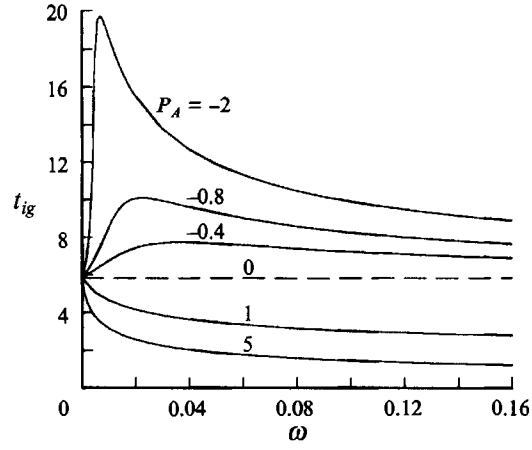

FIGURE 3. Plot of the ignition time t_{ig} as a function of ω for several values of P_A and for $\beta_T = 0$. The dashed curve corresponds to the results of Linan & Crespo (1976). Pulse pressure profile.

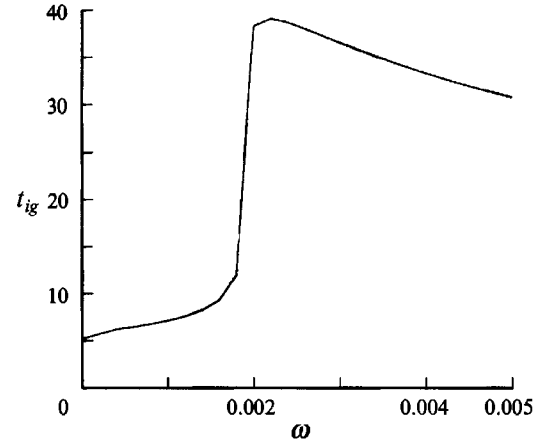

FIGURE 4. Plot of the ignition time t_{ig} as a function of ω for $P_A = -4$ and for $\beta_T = 0$. Pulse pressure profile.

is delayed for negative pressures. In contrast to the previous case, for a positive pressure pulse the ignition time decreases monotonically as ω is increased from zero and asymptotes to a finite non-zero value as $\omega \to \infty$; hence, ignition is enhanced. Since $\beta_T = 0$, ignition takes place along a line parallel to the y-axis located at $z_{ig} = 0$ for any value of P_A and ω. The general behaviour described in figure 3 for $\beta_T = 0$ is seen to hold for any value of β_T, the only exception being the starting value of t_{ig} at $\omega = 0$; for $\beta_T < 0$, the starting value is above that given in the figure, while for $\beta_T > 0$ it is below. In addition, the location of the ignition line resides in the hotter region and moves toward $z = 0$ as ω is increased from zero for fixed P_A.

An interesting feature is seen to occur as P_A is further decreased below -2. This is shown in figure 4 where we plot t_{ig} versus ω for $P_A = -4$ and $\beta_T = 0$. The ignition time increases slowly up to about $\omega \approx 0.0018$, where a sudden jump in t_{ig} occurs. As ω increases still further, the ignition time reaches a maximum and then begins to decay slowly, reaching an asymptote as $\omega \to \infty$. To better explain this jump phenomenon, we plot in figure 5 the maximum of T_1 versus time for several values of ω. Note that there

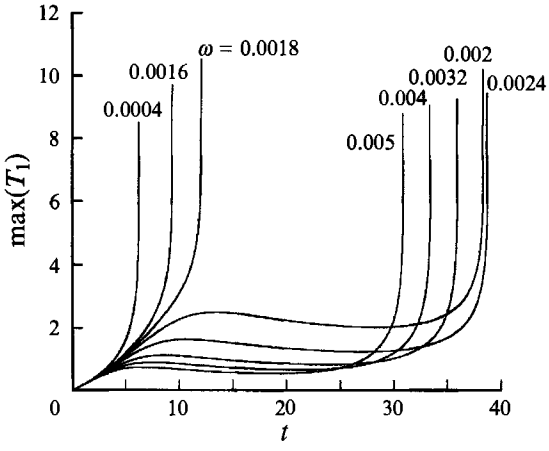

FIGURE 5. Plot of the maximum of the temperature perturbation T_1 as a function of time t for several values of ω and for $P_A = -4$ and $\beta_T = 0$. Pulse pressure profile.

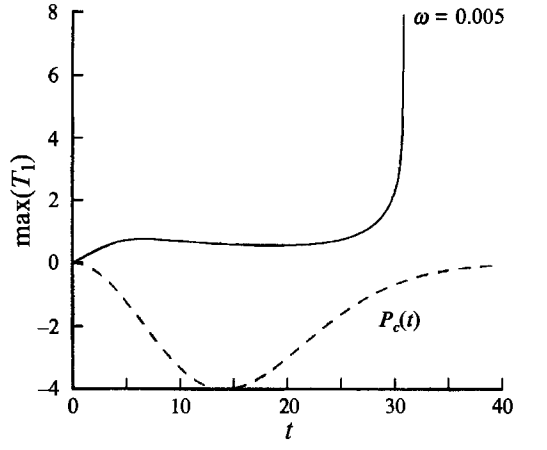

FIGURE 6. Plot of the maximum of the temperature perturbation T_1 as a function of time for $\omega = 0.005$, $P_A = -4$, and $\beta_T = 0$. The dashed curve is the pressure profile. Pulse pressure profile.

is a sudden jump in the ignition time between $\omega = 0.0018$ and $\omega = 0.002$. For values of ω below 0.0018, the maximum temperature perturbation is seen to increase monotonically, becoming infinite as t approaches t_{ig}. For values of ω greater than about 0.0018, the maximum temperature perturbation increases at first, decreases slightly, and then increases sharply and becomes unbounded as $t \to t_{ig}$. In the region where the maximum decreases, the pressure disturbance dominates in the exponent of (3.17), yielding a region where the chemical activity is suppressed, and so the temperature evolves according to a homogeneous heat equation; this parallels that of the linear pressure case. However, unlike the linear pressure case, the pulse does not grow unbounded, but instead reaches a minimum and then increases back to zero. Thus, there exists some finite time at which the pressure no longer dominates the exponent, and the problem begins to once again evolve according to classical thermal explosion theory. A comparison of the pressure pulse and maximum temperature perturbation is provided in figure 6 for one selected value of ω. Note that the maximum in T_1 decreases over most of the pressure pulse, and that the temperature again rises

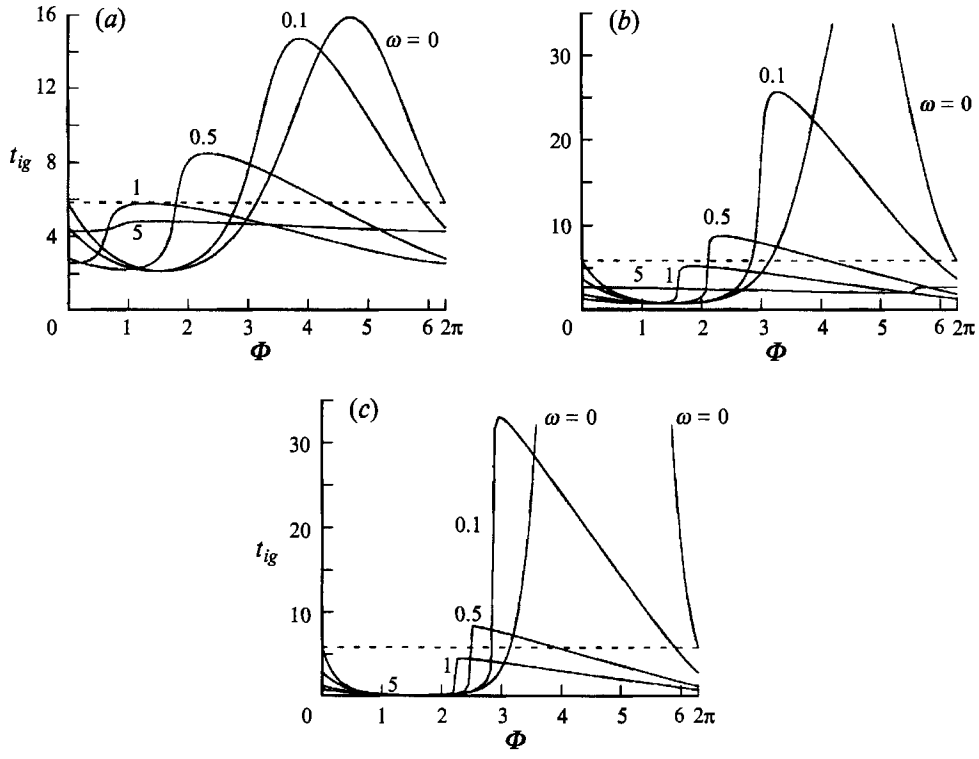

FIGURE 7. Plot of the ignition time t_{ig} as a function of phase Φ for several values of the frequency ω and for $\beta_T = 0$: (*a*) $P_A = 1$; (*b*) $P_A = 2$; (*c*) $P_A = 4$. The dashed curve corresponds to the results of Linan & Crespo (1976). Sinusoidal pressure profile.

once the pressure increases to some critical value. Finally, we note here that the above behaviour was seen to occur numerically for all pressure amplitudes less than about -2.8, and also occurs for non-zero values of β_T.

3.1.3. *Sinusoidal pressure variation*

Let the flow be subject to a sinusoidal pressure variation at $t = 0$ of the form

$$P_c(t) = P_A \sin(\omega t + \Phi), \tag{3.21}$$

where $\omega > 0$ is the frequency, P_A is the amplitude, and Φ is the phase of the pressure variation. This profile was chosen since it can be regarded as a single Fourier mode of a more general pressure disturbance. Figure 7(*a–c*) is plots of t_{ig} versus the phase angle Φ for $P_A = 1, 2, 4$, respectively, and for various values of ω with $\beta_T = 0$. The case of $P_A = 0$ corresponds to that of Linan & Crespo (1976) and is shown in each figure as a dashed line for reference. We begin by noting that there are several important features which are common to all three figures. These are: (i) the maximum ignition time at a fixed amplitude corresponds to zero frequency with a phase angle greater than π (corresponding to an initial negative pressure wave), and that this maximum decreases and shifts to lower phase angles as ω is increased from zero; (ii) for frequencies $\omega \approx 1$ and greater, the ignition time always lies below that of the dashed line for any phase angle and amplitude, indicating that ignition is enhanced over the zero-pressure-disturbance case; and (iii) for the high-frequency range ($\omega > 5$), the ignition time is

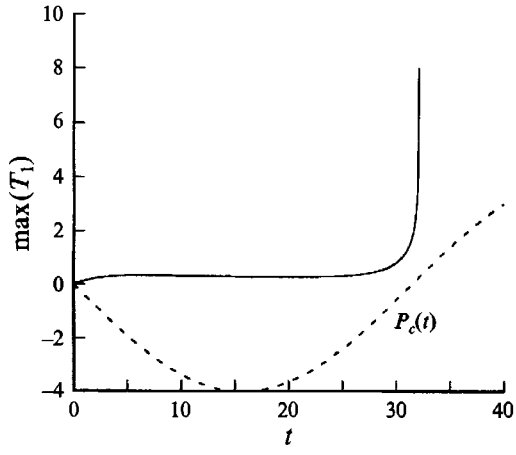

FIGURE 8. Plot of the maximum of the temperature perturbation T_1 as a function of time for $P_A = 4$, $\omega = 0.1$, $\Phi = \pi$, and $\beta_T = 0$. The dashed curve is the corresponding sinusoidal pressure profile.

approximately a constant over the entire range of phase angles, and that this constant value decreases as the pressure amplitude P_A increases.

The same interesting feature that occurred for the pressure-pulse case is also seen to occur for the sinusoidal-pressure case, namely that the ignition time undergoes a sudden jump in its value for certain combinations of amplitude, frequency, and phase. The jump phenomenon in the ignition time is clearly shown in figure 7(*c*) for $P_A = 4$. For the curves $\omega \geqslant 0.1$, the ignition time drops slowly as Φ is increased from zero, reaches a minimum, and then begins to increase slowly as Φ is increased further until a critical value of Φ is reached, where the ignition time then undergoes a sudden jump in its value. As Φ increases still further, the ignition time reaches a maximum and then begins to decrease back to its original value at $\Phi = 0$. To better explain this jump phenomenon, we plot in figure 8 the maximum of T_1 versus time for $P_A = 4$, $\omega = 0.1$ and $\Phi = \pi$. The corresponding pressure wave is displayed as the dashed curve. In the region where the maximum temperature perturbation is almost constant, the pressure perturbation dominates in the exponent of (3.17) yielding a region where the chemical activity is suppressed, and so the temperature evolves according to a homogeneous heat equation, and ignition is delayed. As the pressure rises to some critical value, chemical activity resumes and ignition soon takes place according to classical thermal explosion theory.

Figure 9(*a*, *b*) shows that regions of chemical inactivity can exist in the ignition regime even in the high-frequency limit. Figure 9(*a*) shows the maximum of T_1 as a function of time for $P_A = 2$, $\omega = 5$, and $\Phi = \pi/10$, while figure 9(*b*) is a similar graph except now $\omega = 10$. In each graph, the corresponding pressure variation is shown as a dashed curve. Note that there are now several regions where the maximum temperature perturbation decreases and hence chemical activity is suppressed, with the pressure variation being negative in each of those regions.

Finally, we note here that the general behaviour described in figures 7–9 for $\beta_T = 0$ is seen to occur for any value of β_T. The only exception being that for $\beta_T < 0$ the ignition time is greater than that given for $\beta = 0$, while for $\beta_T > 0$ it is less.

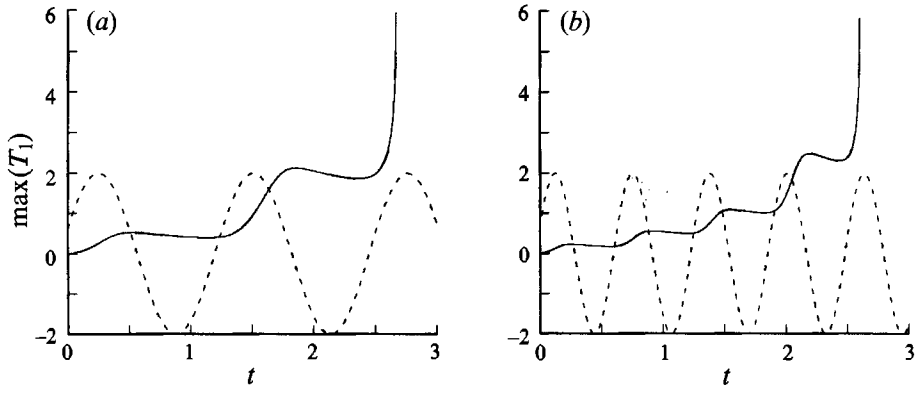

FIGURE 9. Plot of the maximum of the temperature perturbation T_1 as a function of time for $P_A = 2$, $\Phi = \pi/10$, $\beta_T = 0$. The dashed curve is the corresponding sinusoidal pressure profile. (*a*) $\omega = 5$; (*b*) $\omega = 10$.

3.2. $R > 0$

When vortical motion is taken into account, the governing reactive convection-diffusion equations for the temperature and mass fraction perturbation are

$$T_{1,t} + \frac{R\,Sc}{r^2}[1 - e^{(-r^2/4tSc)}]\,T_{1,\theta} = \nabla^2 T_1 + \phi F_1^I F_2^I e^{T_1 + P_c(t)}, \tag{3.22}$$

$$F_{j,t}^I + \frac{R\,Sc}{r^2}[1 - e^{(-r^2/4tSc)}]\,F_{j,\theta}^I = \nabla^2 F_j^I, \quad j = 1, 2, \tag{3.23}$$

subject to the conditions (3.10). This system was solved numerically for a range of R, $\beta_T = 0$, $Sc = \phi = 1$, and with an assumed form for the pressure variation term $P_c(t)$. Implementation of boundary conditions is facilitated if the system is recast in Cartesian coordinates. The solution technique is a second-order finite difference scheme on a non-uniform mesh. To resolve the structure in the core region of the field, a coordinate stretching is used. To avoid the singularity at the origin, no mesh points are placed there. The outer boundaries are set at 50 or 200 in the y-direction, and 20 or 50 in the z-direction. Grid resolution studies which at least doubled the computational mesh were carried out to ensure that structures were well resolved. The resolutions required ranged from a 64^2 mesh to a 256^2 mesh for large vortex Reynolds number. The time-stepping scheme is of four-stage Runge–Kutta type which is formally second-order but has an extended stability region making it accurate and robust for moderately stiff problems. All runs were performed on a Cray YMP.

As t increases, the solution for T_1 becomes unbounded at some finite time (t_{ig}) and location (y_{ig}, z_{ig}). This characterizes the ignition regime. The special case $R = 0$, in which two initially unmixed species are allowed to diffuse without the mixing generated by the vortex, has been presented in §3.1. For this case, ignition takes place along a line parallel to the y-axis which is located at $z_{ig} = 0$ for $\beta_T = 0$ and residues in the hotter region for $\beta_T \neq 0$. For $R > 0$, previous work (Macaraeg *et al.* 1992) has shown, in the absence of a pressure disturbance, that ignition occurs at a point rather than along an entire line. The ignition point is located at the origin for $\beta_T = 0$ and for any value of R, and in the hotter region for $\beta_T \neq 0$. For $\beta_T \neq 0$, the ignition location spirals clockwise towards the viscous core centre as R is increased from zero, with ignition taking place within the core for $R > 70$.

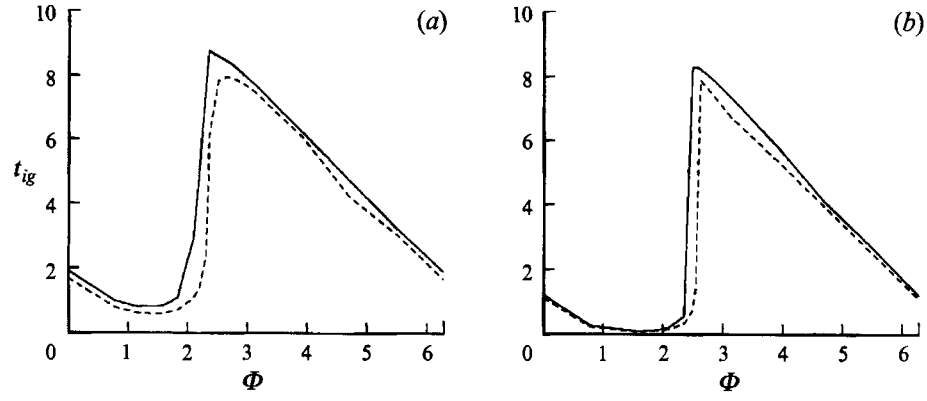

FIGURE 10. Plot of the ignition time versus phase Φ for (*a*) $P_A = 2$ and (*b*) $P_A = 4$ with $\omega = 0.5$ and for vortex Reynolds number $R = 0$ (solid) and $R = 100$ (dashed).

To determine the combined effects of the vortex and a pressure disturbance on the ignition time, we produce here selected results using the sinusoidal pressure function (3.21) for $P_c(t)$. In all calculations, we fix $Sc = \phi = 1$ and $\beta_T = 0$, and vary the parameters P_A, R, ω, and Φ. Since $\beta_T = 0$ and $R > 0$, ignition will occur in the vortex centre. Figure 10(*a*, *b*) is plots of t_{ig} versus the phase angle Φ for $P_A = 2$ and 4, respectively, and for vortex Reynolds number $R = 0$ (solid) and $R = 100$ (dashed) with $\omega = 0.5$. The results with $R = 0$ (solid) are taken from figure 7 and given here as a reference when $R > 0$. From figure 10 we see that the effect of increasing R is to decrease slightly the ignition time for any phase. This is consistent with previous results obtained when pressure disturbances were ignored (Macaraeg *et al.* 1992).

To illustrate the structure in the high-frequency limit, we plot in figures 11(*a*) and 11(*b*) the maximum of the temperature perturbation T_1 as a function of time for $\omega = 5$ and 10, respectively, and for various values of the vortex Reynolds number R with $P_A = 2$, $\Phi = \pi/10$, and $\beta_T = 0$. The special case of $R = 0$ was previously shown in figure 9 and is used here as a reference case for when $R > 0$. In both figures, the structure is similar to the $R = 0$ case, except that increasing R decreases the ignition time slightly until about $R = 100$, when the ignition time remains constant as R is increased further. As stated earlier, the temperature maximum always occurs in the vortex centre.

3.3. *Approximation for the ignition time*

Since a certain amount of mixing must take place before ignition, a surprisingly good approximation to the ignition time in the presence of a pressure disturbance can be found by considering the 'homogeneous' problem

$$\frac{dT_1}{dt} = \frac{1}{t_{ig}^O} e^{T_1 + P_c(t)}, \tag{3.24}$$

where the factor t_{ig}^O is the ignition time in the absence of a pressure disturbance chosen to be the Linan & Crespo (1976) result, which accounts for the role that diffusion plays in the mixing of the reactants as well as the role that the initial temperature profile plays. For $\beta_T = -2$, 0, and 2, we find that $t_{ig}^O = 13.1961$, 5.8285, and 1.7736, respectively, for our choice of the timescales (3.4). Integrating (3.24), we find that

$$T_1 = -\ln\left[1 - \frac{1}{t_{ig}^O}\int_0^t e^{P_c(\tau)}\, d\tau\right]. \tag{3.25}$$

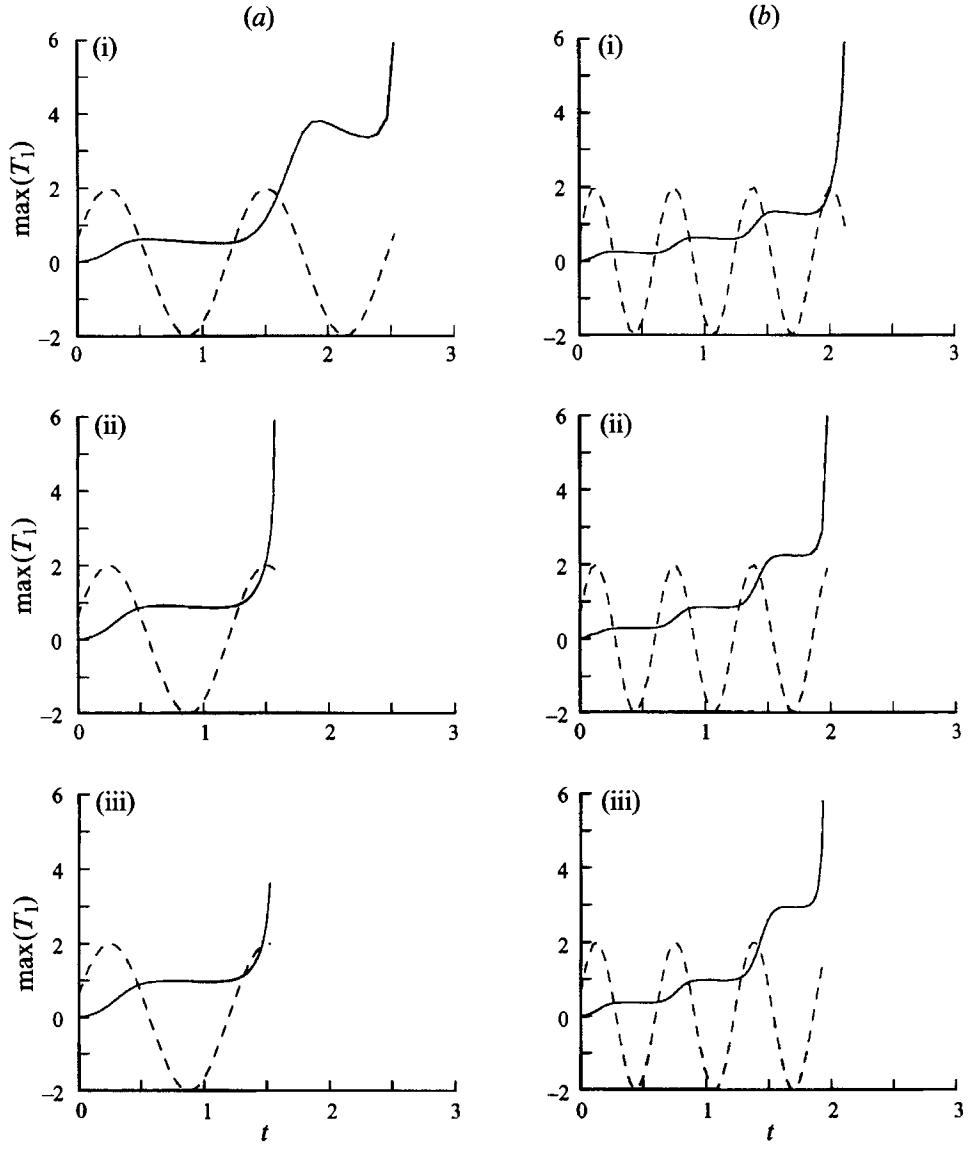

FIGURE 11. Plot of the maximum temperature perturbation T_1 as a function of time for (*a*) $\omega = 5$, and (*b*) $\omega = 10$ with $P_A = 2$, $\Phi = \pi/10$, $\beta_T = 0$ and for (i) $R = 10$, (ii) $R = 50$, and (iii) $R = 100$. The dashed core is the corresponding sinusoidal pressure profile.

Ignition takes place when the quantity in square brackets of (3.25) vanishes; that is, the 'homogeneous' ignition time t_{ig}^H is given implicitly by the equation

$$\int_0^{t_{ig}^H} e^{P_c(\tau)}\, d\tau = t_{ig}^O. \tag{3.26}$$

In the absence of a pressure disturbance, $P_c(t) = 0$ and therefore $t_{ig}^H = t_{ig}^O$. Below we give selected comparisons between the ignition times predicted by this 'homogeneous' theory and by the full numerical solutions of the previous subsections.

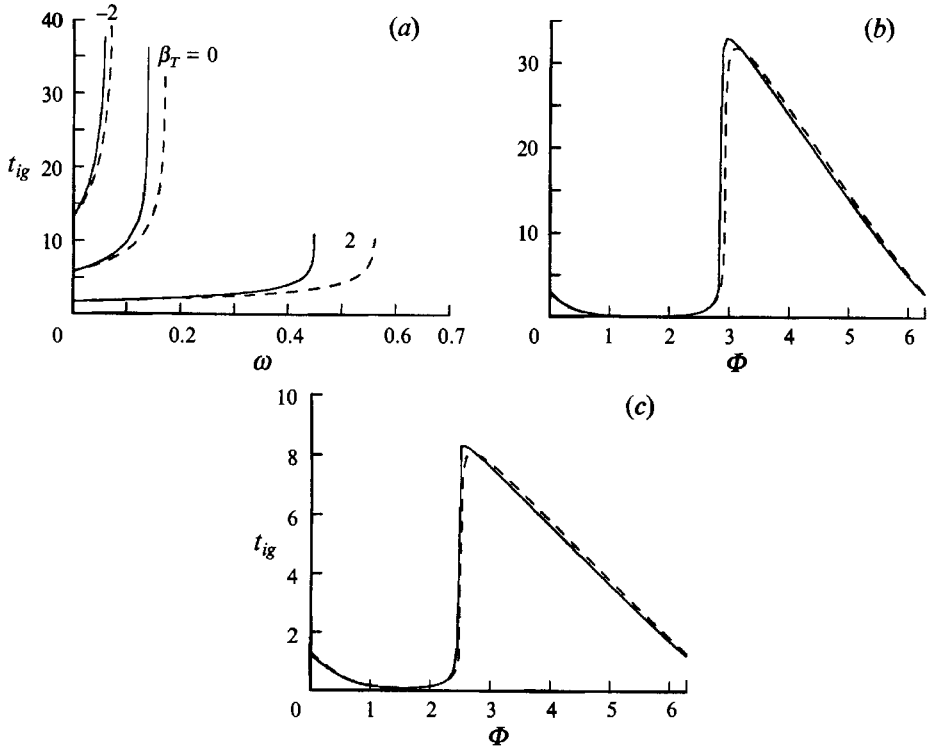

FIGURE 12. Plot of the ignition times corresponding to the full numerical solutions (solid) and the 'homogeneous' ignition times (dashed) as a function of (*a*) ω using the linear pressure profile; (*b*) phase Φ using the sinusoidal pressure profile with $P_A = 4$ and $\omega = 0.1$; and (*c*) phase Φ using the sinusoidal pressure profile with $P_A = 4$ and $\omega = 0.5$.

First, consider the simple linear pressure profile given by (3.19). Substitution into (3.26) yields for the approximate ignition time

$$t_{ig}^H = \frac{-1}{\omega} \ln [1 - \omega t_{ig}^O]. \tag{3.27}$$

Note that (3.27), in addition to defining the approximate ignition time, also approximates the critical value of ω for which ignition can take place. That is, ignition occurs for $0 \leqslant \omega < \omega_c^H$, where $\omega_c^H = 1/t_{ig}^O$ is the critical value; for $\omega > \omega_c^H$, ignition does not take place. In figure 12(*a*) we plot the ignition times for the numerical solutions of §3.1.1 (solid) and the approximate solutions (dashed) for $\beta_T = -2$, 0, and 2 as a function of ω. For each β_T, note that the approximate ignition times compare rather well to those obtained from the full solutions. Now compare the sinusoidal pressure function given by (3.21). For this case, (3.26) must be solved implicitly for t_{ig}^H for fixed values of P_A, ω, Φ and β_T. In figure 12(*b*, *c*) we plot the ignition times for the numerical solutions of §3.1.3 (solid) and the approximate solutions (dashed) as a function of phase Φ and for $P_A = 4$, $\omega = 0.1$ and $P_A = 4$, $\omega = 0.5$, respectively, with $\beta_T = 0$. In each figure note how well the approximate ignition times compare to the ignition times of the full numerical problem. Thus, we see that our theory of homogeneous ignition predicts surprisingly well the true ignition times. Finally, we note here that our definition of the homogeneous ignition time can also be used to predict ignition when vortical motion is present, since ignition times vary little with vortex Reynolds number R.

4. Direct numerical simulation

To investigate post-ignition events up to the development of a flame sheet, the direct numerical solution to (2.3) is necessary. Unfortunately, as mentioned above, the numerical solution of the full system (2.3) presents a formidable task. One approximation which will simplify (2.3) to a more tractable system and has often appeared in the literature is the assumption of small heat release (e.g. Matkowsky & Sivashinsky 1979; Van Harten *et al.* 1984). The resulting system can then be solved numerically. We begin the analysis of small heat release by assuming $\beta \ll 1$. The temperature and density must now be rescaled according to

$$T \to 1 + \beta(T + P_c(t)), \quad \rho \to 1 + \beta\rho, \tag{4.1}$$

while the other variables remain unchanged. To leading order in β, the system (2.3) reduces to

$$T_t + \frac{RSc}{r^2}[1 - e^{-r^2/4tSc}]\, T_\theta = \nabla^2 T + \phi\lambda^{-1} F_1 F_2 e^{\lambda(T+P_c(t))}, \tag{4.2}$$

$$F_{j,t} + \frac{RSc}{r^2}[1 - e^{-r^2/4tSc}]\, F_{j,\theta} = \nabla^2 F_j - \phi\lambda^{-1} F_1 F_2 e^{\lambda(T+P_c(t))}, \quad j = 1, 2, \tag{4.3}$$

for the temperature and mass fractions, while the leading-order solution to the continuity and momentum equations (2.3*b–e*) is the incompressible vortex solution (3.5)–(3.7). The density can be found from the gas law. In the above equations, $\lambda = \beta Ze$ is the product of the heat release parameter and Zeldovich number, $\delta = \beta\gamma/(\gamma - 1)$, and (3.4) with $A = \phi$ has been used in the definition of the Damköhler number. Finally, we note here that by using the definition (4.1) for the temperature, we have subtracted out the time-varying part due to pressure fluctuations; that is, if T oscillates at any point in the flow field, it will be due solely to the nonlinear source term in (4.2).

The system (4.2)–(4.3) must be solved numerically subject to the boundary and initial conditions

$$T = 0, F_1 = 1, F_2 = 0 \quad \text{at} \quad t = 0, r > 0, 0 < \theta < \pi \quad \text{and} \quad t > 0, r \to \infty, 0 < \theta < \pi, \tag{4.4a}$$

$$T = \beta_T, F_1 = 0, F_2 = \phi^{-1} \quad \text{at} \quad t = 0, r > 0, \pi < \theta < 2\pi \quad \text{and} \quad t > 0, r \to \infty, \pi < \theta < 2\pi. \tag{4.4b}$$

This system was solved by the finite difference scheme mentioned in §3. To illustrate the numerical solution of the continuous evolution from nearly frozen flow to near-equilibrium flow, we produce here selected results using the sinusoidal pressure function (3.21) for $P_c(t)$. In all calculations we take $Sc = \phi = 1$ and $\beta_T = 0$.

To investigate the combined effects of a pressure disturbance and of vortical motion on the structure of the full solution, we begin by examining the structure in the absence of these effects. Figure 13(*a*) is a plot of the maximum values of T as a function of time for $R = 0$, $P_c(t) = 0$ and $\lambda = 1$, 0.1 and 0.01. Since $\beta_T = 0$ and $R = 0$, this maximum occurs along the line $z = 0$. For $\lambda = 1$, the temperature increases gradually from zero at $t = 0$ to $T = 0.5$ as $t \to \infty$, this maximum value corresponding to the flame sheet value given in the next section. As λ decreases from one, the rise in temperature near $t = 0$ increases sharply, indicating the existence of a well-defined ignition regime. An interesting trend develops if pressure fluctuations are now included. In figure 13(*b*) we plot the maximum values of the temperature as a function of time for $R = 0$ and for

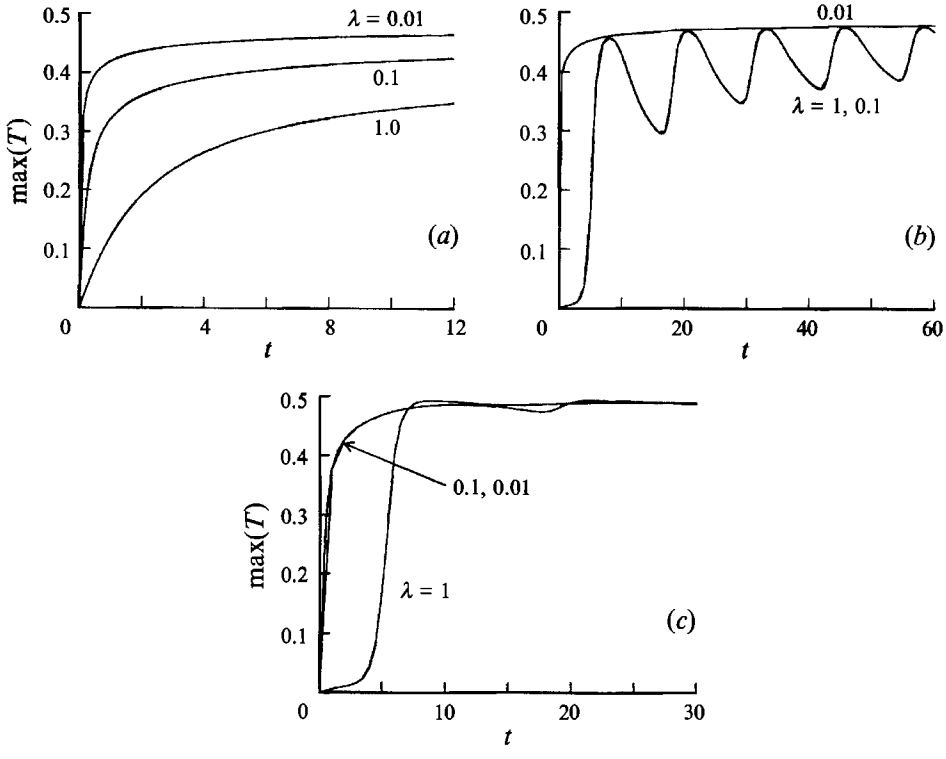

FIGURE 13. Plot of the maximum temperature T as a function of time for $\lambda = 1, 0.1, 0.01$, and for (*a*) $P_e(t) = 0$ and $R = 0$; (*b*) $P_A = 4$, $\omega = 0.5$, $\Phi = 1.25\pi$, and $R = 0$; and (*c*) $P_A = 4$, $\omega = 0.5$, $\Phi = 1.25\pi$, and $R = 50$.

the sinusoidal pressure function (3.21) with $P_A = 4$, $\omega = 0.5$ and $\Phi = 1.25\pi$. For $\lambda = 1$ and 0.1, the temperature rises from $t = 0$ to a maximum value slightly below the flame sheet value of 0.5, and then begins to oscillate in time with decreasing amplitude; as $t \to \infty$, the oscillations die out and the temperature maximum approaches the value 0.5. As λ is decreased from 0.1 to 0.01, ignition takes place so rapidly that the acoustic field is seen to have almost no effect on the temperature field. The absence of any effect due to pressure disturbance is consistent with the flame sheet solution presented in the following section. A surprising phenomenon occurs when vortical motion is included. In figure 13(*c*) we again plot the maximum values of the temperature as a function of time, again for $\lambda = 1$, 0.1 and 0.01, with $R = 50$ and the same pressure profile as in figure 13(*b*). Since $\beta_T = 0$ and $R > 0$, this maximum occurs in the vortex centre. Note that for all three values of λ, the temperature profile evolves in time with little influence from the pressure field. That is, the temperature within the viscous core, once it reaches a maximum, remains almost constant with time, indicating that viscous effects damp out the acoustics. In contrast, we show in figure 14 the maximum temperature at the origin (solid) and the maximum temperature far away from the core (dashed) as a function of time for the same conditions as in figure 1(*c*) with $\lambda = 1$. From this figure we see that, although the temperature within the core remains almost constant with time, the outer flow is oscillating. This is consistent with figure 13(*b*), since the outer flow does not feel the influence of the vortex so that the acoustic field has a noticeable effect. Finally, the oscillations in the outer flow will eventually die out, consistent with the flame sheet solution given in the next section.

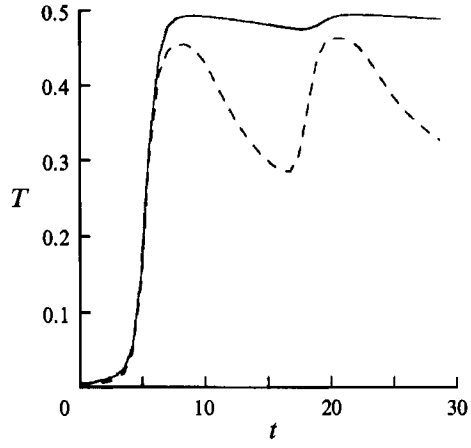

FIGURE 14. Plot of the maximum temperature T at the vortex centre (solid) and far away from the vortex centre (dashed) as a function of time, with $\lambda = 1$, $P_A = 4$, $\omega = 0.5$, $\Phi = 1.25\pi$, and $R = 50$.

5. Diffusion flame regime

After ignition has taken place, a thin diffusion flame exists and is characterized by a chemical reaction time that is much smaller than a characteristic diffusion time. Chemical reactions then occur in a narrow zone between the fuel and the oxidizer, where the concentrations of both reactants are very small. Mathematically, the assumption of very fast chemical reaction rates leads to the limit of infinite Damköhler number, which reduces the diffusion flame to a flame sheet (i.e. local chemical equilibrium). This assumption significantly reduces the complexity of the problem since it eliminates the analysis associated with the chemical kinetics. For many flows, the assumption of local chemical equilibrium adequately predicts the location and the shape of the diffusion flame (Buckmaster & Ludford 1982; Williams 1985). For finite values of the Damköhler number, (4.2) must be solved numerically; and this was done in the previous section.

We begin the description of the diffusion flame regime by defining the following conserved variables (see e.g. Williams 1985):

$$T+F_1 = \beta_T+(1-\beta_T)Z, \tag{5.1}$$

$$T+F_2 = (\beta_T+\phi^{-1})(1-Z), \tag{5.2}$$

$$Z = \frac{F_1-F_2+\phi^{-1}}{1+\phi^{-1}}, \tag{5.3}$$

where Z is the mixture mass fraction and satisfies the convection–diffusion equation

$$Z_t+\frac{RSc}{r^2}[1-e^{-r^2/4tSc}]Z_\theta = \nabla^2 Z, \tag{5.4}$$

subject to the initial and boundary conditions

$$Z = 1 \quad \text{at} \quad t = 0, r > 0, 0 < \theta < \pi \quad \text{and} \quad t > 0, r \to \infty, 0 < \theta < \pi, \tag{5.5a}$$

$$Z = 0 \quad \text{at} \quad t = 0, r > 0, \pi < \theta < 2\pi \quad \text{and} \quad t > 0, r \to \infty, \pi < \theta < 2\pi. \tag{5.5b}$$

In the limit $\lambda \to 0$ (i.e. infinite Damköhler number) the flame-sheet solution is given by

$$F_1 = 1-(1+\phi^{-1})(1-Z), \quad F_2 = 0, \tag{5.6a}$$

$$T = (\beta_T+\phi^{-1})(1-Z), \tag{5.6b}$$

valid for $Z > Z_f$, and $$F_1 = 0, \quad F_2 = \phi^{-1} - (1+\phi^{-1})\,Z, \tag{5.7a}$$

$$T = \beta_T + (1-\beta_T)\,Z, \tag{5.7b}$$

valid for $Z < Z_f$. Here, Z_f defines the location of the flame sheet where both the reactants vanish, given by the implicit relation

$$Z_f = \frac{1}{1+\phi}, \tag{5.8a}$$

and T takes the adiabatic flame value

$$T_f = \frac{1+\beta_T\phi}{1+\phi}. \tag{5.8b}$$

Note that the flame location is independent of β_T and β. Once $Z = Z(r, \theta, t)$ is known, then the other variables (T, F_1, F_2) can be found from (5.6)–(5.7). We remark here that if $\beta_T = 0$ and $\phi = 1$, then $T_f = 0.5$, which is consistent with figures 13 and 14. We also note that the flame-sheet structure and position is independent of the pressure disturbance $P_c(t)$, again consistent with figures 13 and 14 in the limit $t \to \infty$.

As mentioned in the Introduction, equation (5.4) for Z is exactly Marble's (1985) problem when ignition events are ignored (i.e. the vortex is turned on at $t = 0$ with the initial configuration given by the flame sheet), though derived for order-one heat release and with the constant-density approximation, and was solved numerically by Laverdant & Candel (1988) and Rehm *et al.* (1989).

6. Conclusions

The problem of a flame interacting with a vortex is assumed to model certain fundamental mechanisms of turbulent diffusion flames which form the basis of many propulsion devices. Acoustic waves are always present in these combustion systems, so that it is important to study the role of acoustics in such flame/vortex interactions. Having said this, we refrain from any further comment on the implications of the present study to practical applications.

The present study assumes a one-step, irreversible Arrhenius reaction between initially unmixed species occupying adjacent half-planes which are allowed to mix and react by convection and diffusion in the presence or absence of a vortex, and investigates the influence of the acoustic field (spatially uniform but time-dependent pressure waves of small amplitude) on the ignition time and flame structure which are functions of vortex Reynolds number, initial temperature difference of the reactants, equivalence ratio and Schmidt numbers.

In the case of zero vortex Reynolds number and near-equal initial temperatures of the reactants, this study concludes that the low-frequency pressure waves accelerate or decelerate ignition depending on the phase; the pressure waves with moderate to high frequencies always enhance ignition and are essentially independent of phase. Another key result is that the simple theory of homogeneous ignition developed in this study is found to predict these trends very well, and therefore it is proposed as a good engineering approximation for obtaining the ignition times for the more complicated flow fields. When vortical motion was included, the overall ignition time decreases slightly and then asymptotes to a finite value with increasing vortex Reynolds number, consistent with previous results obtained by ignoring acoustics (Macaraeg *et al.* 1992). While the asymptotic analysis is confined to incipient ignition, a direct numerical

simulation is carried out to investigate post-ignition events. This is limited by the small-heat-release assumption. Relaxing this rather drastically restrictive assumption is worth a serious attempt. An important conclusion from the numerical investigation is that acoustics has little effect on the flow field in the vortex core, while the flow outside the core oscillates. It is believed that viscosity in the reacted core damps out the acoustic field.

The authors are grateful to the referees and to D. G. Lasseigne (Old Dominion University) for their helpful comments, whose remarks have improved the paper.

T.L.J. and M.Y.H. were supported by the National Aeronautics and Space Administration under NASA Contract No. NAS1-18605 while in residence at the Institute for Computer Applications in Science and Engineering, NASA Langley Research Center, Hampton, VA 23681-0001. T.L.J. was also supported in part by AFOSR Contract 91-0180.

REFERENCES

BUCKMASTER, J. 1992 Flame stability. In *Major Research Topics in Combustion* (ed. M. Y. Hussaini, A. Kumar & R. G. Voigt), pp. 103–130. Springer.

BUCKMASTER, J. D. & LUDFORD, G. S. S. 1982 *Theory of Laminar Flames*. Cambridge University Press.

BUCKMASTER, J. D. & MATALON, M. 1988 Anomalous Lewis number effects in tribrachial flames. In *Twenty-Second Symp. (Intl) on Combustion*, pp. 1527–1535. The Combustion Institute.

CLARKE, J. F. 1981 Propagation of gasdynamic disturbances in an explosive atmosphere. *Prog. Astron. Aeron.* **76**, 382.

CLARKE, J. F. 1985 Finite amplitude waves in combustion gases. In *The Mathematics of Combustion* (ed. J. D. Buckmaster), pp. 183–245. SIAM.

CORCOS, G. M. 1988 The role of cartoons in turbulence. In *Perspectives in Fluid Mechanics* (ed. D. Coles). Lecture Notes in Physics, vol. 320, pp. 48–65. Springer.

DOLD, J. W. 1989 Flame propagation in a nonuniform mixture: analysis of a slowly varying triple flame. *Combust. Flame* **76**, 71–88.

GOLDSTEIN, M. E. & HULTGREN, L. 1989 Boundary layer receptivity to longwave freestream disturbances. *Ann. Rev. Fluid Mech.* **21**, 137–166.

GROSCH, C. E. & JACKSON, T. L. 1991 Ignition and structure of a laminar diffusion flame in a compressible mixing layer with finite rate chemistry. *Phys. Fluids* A **3**, 3087–3097.

HARTLEY, L. J. & DOLD, J. W. 1991 Flame propagation in a nonuniform mixture: analysis of a propagating triple-flame. *Combust. Sci. Tech.* **80**, 23–46.

JACKSON, T. L. & HUSSAINI, M. Y. 1988 An asymptotic analysis of supersonic reacting mixing layers. *Combust. Sci. Tech.* **57**, 129–140.

JACKSON, T. L., HUSSAINI, M. Y. & RIBNER, H. S. 1993 Interaction of turbulence with a detonation wave. *Phys. Fluids* A **5**, 745–749.

KAPILA, A. K. 1992 Role of acoustics in combustion instability. In *Major Research Topics in Combustion* (ed. M. Y. Hussaini, A. Kumar & R. G. Voigt), pp. 162–178. Springer.

KASSOY, D. R., KAPILA, A. K. & STEWART, D. S. 1989 *Combust. Sci. Tech.* **63**, 33–43.

LAMB, H. 1932 *Hydrodynamics*, 6th edn. Cambridge University Press.

LAVERDANT, A. M. & CANDEL, S. M. 1988 A numerical analysis of a diffusion flame–vortex interaction. *Combust. Sci. Tech.* **60**, 79–96.

LEDDER, G. & KAPILA, A. K. 1991 The response of premixed flames to pressure perturbations. *Combust. Sci. Tech.* **76**, 21–44.

LEE, J. H. S. 1977 Initiation of gaseous detonation. *Ann. Rev. Phys. Chem.* **28**, 75–104.

LINAN, A. & CRESPO, A. 1976 An asymptotic analysis of unsteady diffusion flames for large activation energies. *Combust. Sci. Tech.* **14**, 95–117.

MACARAEG, M. G., JACKSON, T. L. & HUSSAINI, M. Y. 1992 Ignition and structure of a laminar diffusion flame in the field of a vortex. *Combust. Sci. Tech.* **87**, 363–387.

MAJDA, A. 1984 *Compressible Fluid Flow and Systems of Conservation Laws in Several Space Variables.* Springer.

MARBLE, F. E. 1985 Growth of a diffusion flame in the field of a vortex. In *Recent Advances in Aerospace Sciences* (ed. C. Cassci), pp. 395–413. Plenum.

MATKOWSKY, B. J. & SIVASHINSKY, G. I. 1979 An asymptotic derivation of two models in flame theory associated with the constant density approximation. *SIAM J. Appl. Maths* **37**, 686–699.

MCINTOSH, A. C. 1986 Flame resonance and acoustics in the presence of heat loss. In *Reacting Flows* (ed. G. S. S. Ludford). Lectures in Applied Mathematics, vol. 24, pp. 269–301. Springer.

MCINTOSH, A. C. 1989 The interaction of high frequency low amplitude acoustic waves with premixed flames. In *Non Linear Waves in Active Media* (ed. J. Engelbrecht), pp. 218–231. Springer.

MCINTOSH, A. C. 1991 Pressure disturbances of different length scales interacting with conventional flames. *Combust. Sci. Tech.* **75**, 287–309.

MCINTOSH, A. C. & WILCE, S. A. 1991 High frequency pressure wave interaction with premixed flames. *Combust. Sci. Tech.* **79**, 141–155.

MCKENZIE, J. F. & WESTPHAL, K. O. 1968 Interaction of linear waves with oblique shock waves. *Phys. Fluids* **11**, 2350–2362.

NORTON, O. P. 1983 The effects of a vortex field on flames with finite reaction rates. PhD thesis, California Institute of Technology.

ORAN, E. S. & GARDNER, J. H. 1985 Chemical–acoustic interactions in combustion systems. *Prog. Energy Combust. Sci.* **11**, 253–276.

PEARSON, C. F. & ABERNATHY, F. H. 1984 Evolution of the flow field associated with a streamwise diffusing vortex. *J. Fluid Mech.* **146**, 271–283.

PETERS, N. & WILLIAMS, F. A. 1988 Premixed combustion in a vortex. In *Twenty-Second Symp. (Intl) on Combustion*, pp. 495–503. The Combustion Institute.

REHM, R. G., BAUM, H. R., LOZIER, D. W. & ARONSON, J. 1989 Diffusion-controlled reaction in a vortex field. *Combust. Sci. Tech.* **66**, 293–317.

ROBERTS, J. P. 1978 Amplification of an acoustic signal by a laminar premixed gaseous flame. *Combust. Flame* **33**, 79–83.

SHEPHERD, J. E. & LEE, J. H. S. 1992 On the transition from deflagration to detonation. In *Major Research Topics in Combustion* (ed. M. Y. Hussaini, A. Kumar & R. G. Voigt), pp. 439–487. Springer.

TOONG, T. Y., ARBEAU, P., GARRIS, C. A. & PATUREAU, J. P. 1974 Acoustic–kinetic interactions in an irreversibly reacting medium. In *Fifteenth Symp. (Intl) on Combustion.* pp. 87–100. The Combustion Institute.

URTIEW, R. & OPPENHEIM, A. K. 1966 Experimental observations of the transition to denotation in an explosive gas. *Proc. R. Soc. Lond.* A **295**, 13–28.

VAN HARTEN, A., KAPILA, A. K. & MATKOWSKY, B. J. 1984 Acoustic coupling of flames. *SIAM J. Appl. Maths* **44**, pp. 982–995.

WILLIAMS, F. A. 1985 *Combustion Theory*, 2nd edn. Benjamin/Cummings.

ZANG, T. A., HUSSAINI, M. Y. & BUSHNELL, D. M. 1984 Numerical computations of turbulence amplification in shock–wave interactions. *AIAA J.* **22**, 13–21.